

# Spatial Spectral Modeling for Robust MRSI

Ramin Eslami and Mathews Jacob

**Abstract—** We propose a novel spatial spectral model for the reconstruction of *magnetic resonance spectroscopic imaging* (MRSI) signal. We penalize the compartmentalized spatial total variation norm of the signal to exploit the spatial properties of the metabolite peaks. The spectral signal is modeled as a sparse linear combination of spikes and polynomials to capture the peaks and baseline induced by unsuppressed water and lipids. We also use the high-resolution map of the magnetic field distribution within the slice to model the image acquisition, thus correcting for intra-voxel line shape distortions. The spectral model enables the stable recovery of the signal even in challenging spatial regions, while the spatial model suppresses the spectral leakage from extra-cranial fat and inter-voxel crosstalk. We acquire the MRSI signal using EPSI, while the high-resolution 3-D MRI information is derived using Dixon scans. The reconstruction of phantom and in vivo MRSI data demonstrate a significant improvement in spectral quality and accuracy over classical MRSI schemes.

## I. INTRODUCTION

MRSI is a non-invasive scheme that provides in vivo concentration maps of various brain metabolites. Since many of these metabolites play significant roles in brain tumor, this scheme has considerable potential in the clinical management of brain cancer. The routine clinical use of MRSI is hampered by several factors such as poor spatial and spectral resolution and insufficient spatial coverage. Coupled with the significant dynamic range in metabolite signals and the considerable variation of the magnetic field, the low resolution acquisitions results in several artifacts such as spectral leakage and field-map-induced line shape variations. This often makes the quantitative estimation of metabolite concentrations challenging. The main goal of this work is to overcome these challenges, thus obtaining accurate maps of metabolite peaks.

Several spatially constrained reconstruction schemes were introduced in the past to overcome the spectral leakage. Most of these schemes model the spatial distribution of the metabolite peaks as a linear combination of few basis functions, derived using anatomical constraints. The limited ability of these models to capture the spatial variations exhibited by in vivo scans, especially in the context of lesions, make them ineffective in practical applications. The variation of the magnetic field within the spatial compartments also restrict the utility of these schemes. We model the spatial distribution of the metabolite peaks using a novel compartmentalized total variation penalty, where the spatial compartments are derived from high resolution MRI scans. Specifically, we penalize the  $\ell_1$ -norm of the finite differences of the signal within the spatial compartments; the finite differences across the compartments are omitted from the norm. This enables the signal to vary abruptly at the compartment boundaries, while being piecewise smooth within the spatial regions.

R. Eslami and M. Jacob are with the Department of Biomedical Engineering, University of Rochester, Rochester, NY 14627 (e-mails: reslami@ieee.org and mathews.jacob@rochester.edu).

This work is partially supported by the University of Rochester's Clinical and Translational Sciences award, Grant number U11RR024160.

An alternate approach to minimize spectral leakage is PRESS volume selection or saturation bands. However, these schemes significantly reduce the spatial coverage, restricting the visualization of spectra from regions close to the brain surface. Most of the current schemes ignore the effect of field-map-induced line shape variations and losses within the reconstruction, in the interest of a simple algorithm. However, this can lead to significant signal losses and line shape variations in voxels, where the field is significantly changing; these variations are often quite significant close to tumors. The ability of quantification algorithms to capture them is rather limited; many of the current methods omit these voxels from further analysis, thus reducing the spatial coverage.

We propose to estimate the field map from high-resolution, 3-D Dixon scans and use them to compensate for these losses. To exploit the high-resolution information, we reconstruct the signal with the same grid spacing as the MRI data; the use of the spatial TV penalty makes the reconstructions well-posed. In spite of the spatial and forward models, the recovery of the spectral peaks on voxels with significant field variations are still challenging. The recovery of the spectral signal, accounting for the field map is analogous to deconvolution. In regions with significant variations, the peaks are significantly blurred, thus making the recovery ill-posed. To further constrain the reconstruction, we model the spectrum as a sparse linear combination of spikes and polynomials. The spikes capture the metabolite peaks, while the polynomials enable the representation of the baseline signal. The novel spectral model significantly aids in the minimization of noise as well as in making the recovery of peaks well-posed.

## II. MRS IMAGE FORMATION

We use the *echo-planar spectroscopic imaging* (EPSI) sequence to scan the object on a Cartesian grid. Ignoring the  $T_1$  relaxation time, we model the MRSI acquisition scheme in the discrete domain as

$$\hat{s}[\mathbf{k}, k_f] = \underbrace{\sum_{\mathbf{n}=\mathbf{0}}^{\mathbf{N}-1} \sum_{n_f=0}^{N_f-1} e^{-j\omega_0(\mathbf{n})k_f} e^{-k_f/T_2^*[\mathbf{n}]} e^{-2\pi(\mathbf{k}\cdot\mathbf{n}+n_fk_f)} v[\mathbf{n}, n_f]}_{\mathcal{A}}, \quad (1)$$

where  $\omega_0 = 2\pi f_0 = \gamma \Delta B_0(\mathbf{r})$  represents the field map in which  $\Delta B_0(\mathbf{r})$  is the field inhomogeneity and  $\gamma$  denotes the gyromagnetic ratio.

Using accompanying MRI scan  $q[\mathbf{n}]$ , we propose to estimate the high-resolution field map and  $T_2^*$  decay. These parameters are estimated using the Dixon scheme, where MRI data is collected at multiple delay times to estimate the field map and fat/water concentrations.

In this paper we consider the MRSI data  $\hat{s}[k_x, k_y, k_f]$  to be at resolution  $(M_x, M_y, N_f)$  and the water-referenced (MRI) data  $q[\mathbf{n}]$  at a higher resolution  $\mathbf{N}=(N_x, N_y, N_z)$ . Note that we assumed same spectral and temporal resolution; i.e.,  $N_f = N_t$ .

### III. MRSI RECONSTRUCTION

#### A. System Model

To exploit the high resolution MRI priors, we propose to reconstruct the MRSI data at the same grid size as the MRI data. Thus, having the scanned MRSI data  $\hat{s}[k_x, k_y, k_f]$  in one slice at resolution  $(M_x, M_y, N_f)$ , we would like to reconstruct  $v[\mathbf{n}, n_f] = v[n_x, n_y, n_z, n_f]$  at a finer grid  $(\mathbf{N}, N_f)$ , which has the same spatial resolution as the estimated field map and  $T_2^*$  decay. As a result, considering the fact that the MR measurements are noisy, we need to solve

$$\|\mathcal{A}v - \hat{s}\| \leq \varepsilon, \quad (2)$$

where  $\mathcal{A}$  indicates the forward (or system) model shown in (1).

As explained in Section 2, in the MR scanner, inhomogeneity and  $T_2^*$  decay affect the desired signal in the temporal domain,  $v_{(f)}$ , through a multiplication by an exponential term. Therefore, to implement  $\mathcal{A}$  we first define the operator  $\mathcal{B}$  as

$$\hat{v}_1[\mathbf{k}, k_f] = \mathcal{B}v[\mathbf{n}, n_f] = \mathcal{F}_{(xyz)} e^{-k_f(1/T_2^*[\mathbf{n}] + j\omega_0[\mathbf{n}])} \mathcal{F}_{(f)} v[\mathbf{n}, n_f]$$

$(\mathbf{0} \leq \mathbf{n} < \mathbf{N}, 0 \leq k_f < N_f)$ ,

where  $\mathcal{F}_{(f)}$  and  $\mathcal{F}_{(xyz)}$  denote the Fourier transform along the spectral and spatial dimensions, respectively. Then we express  $\mathcal{A} = \mathcal{W}\mathcal{B}$  where  $\mathcal{W}$  makes  $\hat{v}_1$  the same size as the measured signal  $\hat{s}$  by picking the center of  $k$ -space at the target size of  $(M_x, M_y, N_f)$ , or  $\hat{v}_2 = \mathcal{W}\hat{v}_1$ .

To exploit the spatial correlation of the MRSI data and to make the reconstruction at a finer grid well-posed, we minimize *total variation* (TV) of  $v[\mathbf{n}, n_f]$  subject to the criterion (2).

We also constrain  $v$  to a mask that covers the field of view  $\Omega$  and constrain the TV norm into two regions of water ( $\Omega_1$ ) and fat ( $\Omega_2 = \Omega - \Omega_1$ ) using the high-resolution scan  $q[\mathbf{n}]$  in order to reduce spectral leakage. (Recall that we also used  $q[\mathbf{n}]$  to estimate the field map.) In general we can add more regions such as CSF, white matter, etc. Thus, we segment the field of view to  $K$  non-overlapping regions  $\Omega = \bigcup_{i=1}^K \Omega_i$ .

Consequently, we propose the following minimization scheme to reconstruct the MRSI data  $v$ :

$$\tilde{v} = \arg \min_v \left\{ \|\mathcal{A}_1 v - \hat{s}\|^2 + \lambda_1 \text{TV}_{\mathbf{n}}^{\Omega}(v) \right\}. \quad (3)$$

In this setting, the updated forward model is defined as  $\mathcal{A}_1 = \mathcal{W}\mathcal{B}\mathcal{M}_{\Omega}$  where  $\mathcal{M}_{\Omega}$  denotes the masking operator to constrain the reconstruction to the field of view:

$$v_{\Omega} = \mathcal{M}_{\Omega} v[\mathbf{n}, n_f] = \begin{cases} v[\mathbf{n}, n_f], & \mathbf{n} \in \Omega; \\ 0, & \text{else} \end{cases};$$

and the constrained TV-norm is defined as  $\text{TV}_{\mathbf{n}}^{\Omega}(v) = \sum_{k=1}^K \|\Delta_{\mathbf{n}}^{\Omega_k} v\|_{\ell_1}$ , where  $\Omega = \{\Omega_1, \dots, \Omega_K\}$  and each spatial constrained gradient is expressed as (definitions for  $y$ - and  $z$ -gradients are similar):

$$\Delta_x^{\Omega_i} v = \begin{cases} v[\mathbf{n} + (1, 0, 0), n_f] - v[\mathbf{n}, n_f]; & \mathbf{n}, \mathbf{n} + (1, 0, 0) \in \Omega_i \\ 0, & \text{else} \end{cases},$$

and we have

$$\|\Delta_{\mathbf{n}}^{\Omega_k} v\|_{\ell_1} = \sum_{\mathbf{n}, n_f} \sqrt{|\Delta_x^{\Omega_k} v|^2 + |\Delta_y^{\Omega_k} v|^2 + |\Delta_z^{\Omega_k} v|^2}.$$

We define the reconstruction error as  $e = \varepsilon \|\hat{s}\|$ . We optimize the regularizing parameter(s) to achieve a desired reconstruction error.

#### B. A New Signal Model

A typical MRSI spectrum, however, is composed of (a) a few metabolite peaks and (b) a baseline due to residual water and fat leakage, and the existence of macromolecules. Therefore, a better model required to represent the MRSI signal. We propose to model the MRSI signal using a union of Diracs and polynomials basis functions  $\Phi = (\varphi \ \psi)$ :

$$v = \Phi w = \underbrace{\varphi w_c}_{\text{base line}} + \underbrace{\psi w_d}_{\text{peaks}}, \quad (4)$$

where  $w = (w_c \ w_d)^T$  represents the coefficients,  $\psi = I$  is the Euclidean (or Dirac) basis that efficiently captures the peaks ( $w_d$ ) while the polynomials  $\varphi$  can represent the baseline. As a consequence, using (4), we propose the new reconstruction scheme as

$$\tilde{w} = \arg \min_w \left\{ \|\mathcal{A}_2 w - \hat{s}\|^2 + \lambda_1 \text{TV}_{\mathbf{n}}^{\Omega}(w) + \lambda_2 \|w\|_{\ell_1} \right\}, \quad (5)$$

where the updated forward model is expressed as  $\mathcal{A}_2 = \mathcal{W}\mathcal{B}\Phi\mathcal{M}_{\Omega}$ . Note that the sparsity constraint does not contradict the smoothness imposed by the spatial TV norm. The TV norm only penalizes the spatial gradients. While used alone as in (3), it does not constrain the signal along the frequency dimension. In contrast, the use of the sparse spectral model constrains the spectral shapes, thus making the recovery of line shapes in regions with significant intra-voxel distortions well-posed. The proposed constrained model opposed to most previous studies [1], [3] exploits the spectral line shapes (peaks and base line) in the reconstruction and provides a sparse representation of the MRSI signal.

Since the piece-wise smooth model is not proper for the fat region in Brain scans, we constrain TV norm in (5) to only the water region ( $\Omega_1$ ); that is we use  $\text{TV}_{\mathbf{n}}^{\Omega_1}(w)$  instead of  $\text{TV}_{\mathbf{n}}^{\Omega}(w)$ .

To achieve baseline decomposition with lower-degree polynomials, we limit their support to a *region of interest* (ROI) where we exclude the water peak.

To represent the baseline, we employ Chebyshev polynomials of the first kind defined as

$$T_0(x) = 1, \quad T_1(x) = x, \\ T_{i+1}(x) = 2xT_i(x) - T_{i-1}(x),$$

for  $x \in [-1, 1]$ . We define the discrete version of the polynomials with a support limited to  $\Lambda = [n_a, n_b]$  as

$$R_i[n] = \begin{cases} T_i \left( \frac{2n - n_a - n_b}{n_b - n_a} \right), & n \in \Lambda \\ 0, & \text{else} \end{cases},$$

and normalize them with their  $\ell_2$ -norm. Thus, we use  $N_p$  polynomials ( $0 \leq i \leq N_p - 1$ ) with limited support as basis functions of  $\varphi$ .

As a result, we can express (4) as

$$v[\mathbf{n}, n_f] = \Phi w = w_d[\mathbf{n}, n_f] + \sum_{i=0}^{N_p-1} w_c[\mathbf{n}, i] R_i[n_f],$$

where  $w_d$  represents the Dirac coefficients and has the same size as  $v$ , whereas  $w_c[\mathbf{n}, i]$  with size  $(\mathbf{N}, N_p)$  denotes the polynomial coefficients using polynomials  $R_i[n]$  of order  $N_p - 1$  and length  $N_f$ .

The TV norm in (5) regularizes the resulting baseline-removed signal  $w_d$  in order to make the line shapes and peaks uniform. This is not attainable by first reconstructing the MRSI signal by using (3) and then removing the base line from each spectral line. Note that the TV norm in (3) applies to the MRSI signal  $v$ , which includes the baseline. Subtracting the varying baseline from the

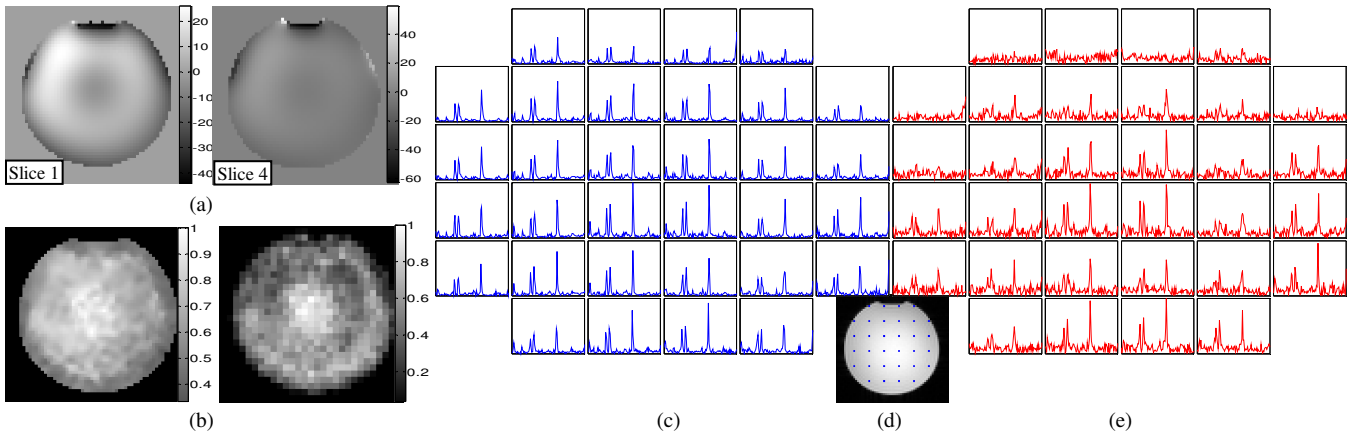


Fig. 1. (a) Field map estimate of the metabolite phantom at slice 1 and slice 4. (b) Reconstructed peak map of Cho in the phantom using the proposed scheme (Left) and the standard scheme (Right). The color bars show the normalized intensity variation within the phantom. (c) A few spectral lines at the voxels shown in (d) reconstructed with the proposed method. (e) Spectra at the same voxels constructed using the standard scheme.

reconstructed  $\tilde{v}$  leads to non-uniformity in the metabolite peaks magnitudes in uniform regions.

An issue in finding the proper solution in regularized minimization schemes is setting the appropriate regularizing parameters, here  $\lambda_1$  and  $\lambda_2$ . Here we attempt to find the appropriate parameters to achieve a desired reconstruction error. Hence, we have one degree of freedom in choosing  $\lambda_1$  and  $\lambda_2$ . In our experience, the parameter  $\lambda_2$  plays the major role in making the problem well-posed. Using a smaller value of  $\lambda_2 \approx 0.1\lambda_1$  is often sufficient to ensure the decomposition of  $v$  into baseline and metabolites components and provide reasonable suppression of artifacts.

#### IV. EXPERIMENTAL RESULTS

We tested our approach for a phantom and in vivo brain data and compared it to the standard scheme [4] integrated with the *Papoulis-Gerchberg* (PG) algorithm [2] as well as the *chemical shift imaging* (CSI) data for the patient brain study. We acquired the water-suppressed MRSI data in a single 10mm-slice with resolution  $(M_x, M_y, N_f) = (64, 32, 256)$  where we used 9 measurements to improve SNR. We chose  $TR = 2$  sec and  $TE = 40$  msec (echo time for the first acquisition) resulting in a total scan time of 10.7 min. We also acquired a water-referenced MRSI data at this resolution to be employed in the standard reconstruction scheme for comparison. We estimated the field map and  $T_2^*$  decay as well as the masks from a higher-resolution  $[(N_x, N_y, N_z) = (128, 64, 4)]$  water data  $q[\mathbf{n}]$  scanned at the same volume as the MRSI scan. For our proposed reconstruction scheme of (5), we employed polynomials of order 7 ( $N_p = 8$ ).

##### A. Uniform Phantom

In the first experiment we used a cylindrical phantom containing water and three metabolites: choline (Cho), creatine (Cr), and N-acetyl-aspartate (NAA). We intentionally selected a slice that included an air bubble on top to have a high inhomogeneity.

We used the regularizing parameters  $\lambda_1 = 0.05$  and  $\lambda_2 = 0.002$  in (5) leading to a reconstruction error of  $e = 5\%$ . In addition to the proposed method, we also used standard reconstruction in which we exploit the water-referenced imaging data acquired at the same resolution as the MRSI data to align the peaks. Then we apply baseline suppression to each spectral line by fitting polynomials of order 7. We also apply spatial apodization at each frequency point  $n_f$  using a 2-D Gaussian window.

Fig. 1(a) depicts the field map estimate of the phantom. As seen, the intensity variation in  $n_z$  is significant which indicates the need

for employing a 3-D field map in the reconstruction. In Fig. 1(b) we demonstrated the reconstructed Cho peak map where the proposed method yields more uniform result. In the standard reconstruction at regions where the inhomogeneity is high, the peaks have small magnitudes close to zero; that is, the MRSI signal is almost lost in those regions (see Fig. 1). This observation is confirmed when we examine the spectra illustrated in Fig. 1(c)-(e). Note that the conventional reconstructions exhibit significant signal intensity variations in spatial regions with significant changes in field map.

##### B. Brain In Vivo Results

###### 1) Healthy Subject

We scanned a slice of the brain of a healthy human and tested our scheme to reconstruct the MRSI signal. We used  $\lambda_1 = 0.05$  and  $\lambda_2 = 0.002$  in (5), which led to a reconstruction error of  $e = 2.3\%$ . For the standard scheme, we used PG algorithm, inhomogeneity correction using the water-referenced scan, baseline removal, and spatial apodization. We used a Gaussian window for the apodization resulting the error of  $e = 5.6\%$ .

Fig. 2(a) and (c) show a few reconstructed spectra at different locations of imaged brain using the proposed scheme and the standard method. While the proposed method yields high quality reconstructed metabolite peaks in all spectra, the reconstructed spectra resulting from the standard method show degraded (sometimes lost) peaks and very noisy line shapes. Note that the remaining fat leakage is comparable for both schemes.

In Fig. 3 we demonstrated the reconstructed NAA peak using different schemes. The proposed method [see Fig. 3(a)] yields the smoothest result, which is not affected by the fat leakage. The standard algorithm [see Fig. 3(c)] shows less smooth result where we observe some oscillatory magnitude variation inside the brain due to fat leakage.

For the TV reconstruction, we also see such oscillatory variation in Fig. 3(b). The high-magnitude boundary regions indicate high-amplitude fat leakage in these areas. These artifacts are not observed in the peak reconstructed using (5), which confirms the use of  $\ell_1$ -norm as well as the new signal model to be appropriate for MRSI brain signals.

###### 2) Patient with Brain Cancer

Finally, we scanned a patient having a tumor using the EPSI sequence as well as the standard CSI sequence available at Siemens Trio 3T MR scanner. The CSI scheme uses the PRESS volume selection to minimize the leakage from lipids. However, this restricts the imaging of voxels close to the brain. Note that many of

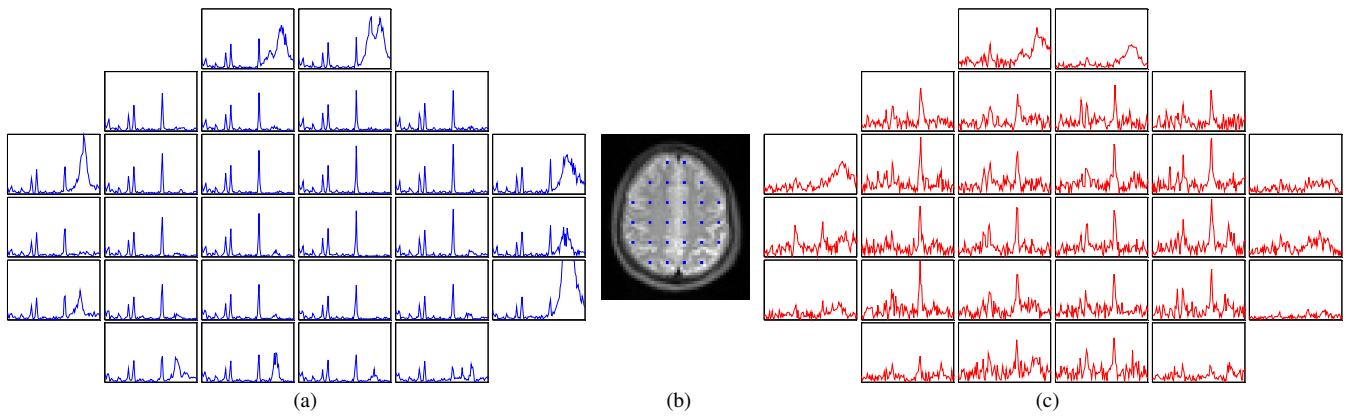


Fig. 2. (a) A few reconstructed spectral lines at voxels shown in (b) using the proposed method. (c) Spectra at the same voxels reconstructed with the standard algorithm.

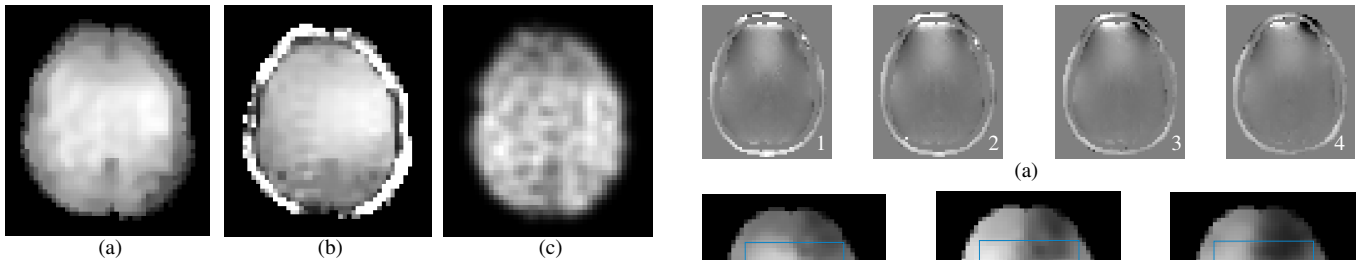


Fig. 3. Reconstructed peak map of NAA using: (a) proposed method [given in (5)], (b) TV reconstruction [given in (3)], and (c) standard method. For cases (b) and (c) baseline removal is applied after reconstruction. Magnitude is clipped for better visualization.

the brain regions close to the tumor cannot be imaged with this scheme. Therefore, the acquired data in the CSI study is valid only over the  $10 \times 8$  voxels shown by a box in Fig. 4(d).

The resulting estimated field map and reconstructions are depicted in Fig. 4. As seen, the peak maps of the metabolites in both methods follow similar patterns. Note that the top row of peak maps of the CSI reconstruction is saturated due to fat leakage and thus is not valid. Lower NAA concentration and relatively higher Cho concentration compared to Cr indicates the tumor in the brain.

A few spectral lines are shown in Fig. 4(c) and (e). The reconstructed peaks using the proposed method are more resolved compared to the spectra of the CSI scheme.

## V. CONCLUSION

In this paper we proposed a new reconstruction scheme for MRSI data. We assumed the MRSI signal is gradient-sparse in the spatial domain and hence applied TV-norm minimization. We also proposed a better signal model for the MRSI signal based on the union of Diracs and polynomials resulting in a sparser signal. We applied the  $\ell_1$ -norm of the decomposed signal to make the problem well-posed and to take advantage of the spectral sparsity. Through several experiments including phantom and in vivo studies we demonstrated improved reconstructions over traditional schemes when using the proposed approach.

## REFERENCES

- [1] J.P. Haldar, D. Hernando, S.-K. Song, and Z.-P. Liang, "Anatomically constrained reconstruction from noisy data," *Mag. Res. Med.*, vol. 59, no. 4, pp. 810-818, Mar. 2008.
- [2] C.I. Haupt, N. Schuff, M.W. Weiner, and A.A. Maudsley, "Removal of lipid artifacts in 1H spectroscopic imaging by data extrapolation," *Mag. Res. Med.*, vol. 35, no. 5, pp. 678-687, May 1996.
- [3] S. Hu *et al.*, "Compressed sensing for resolution enhancement of

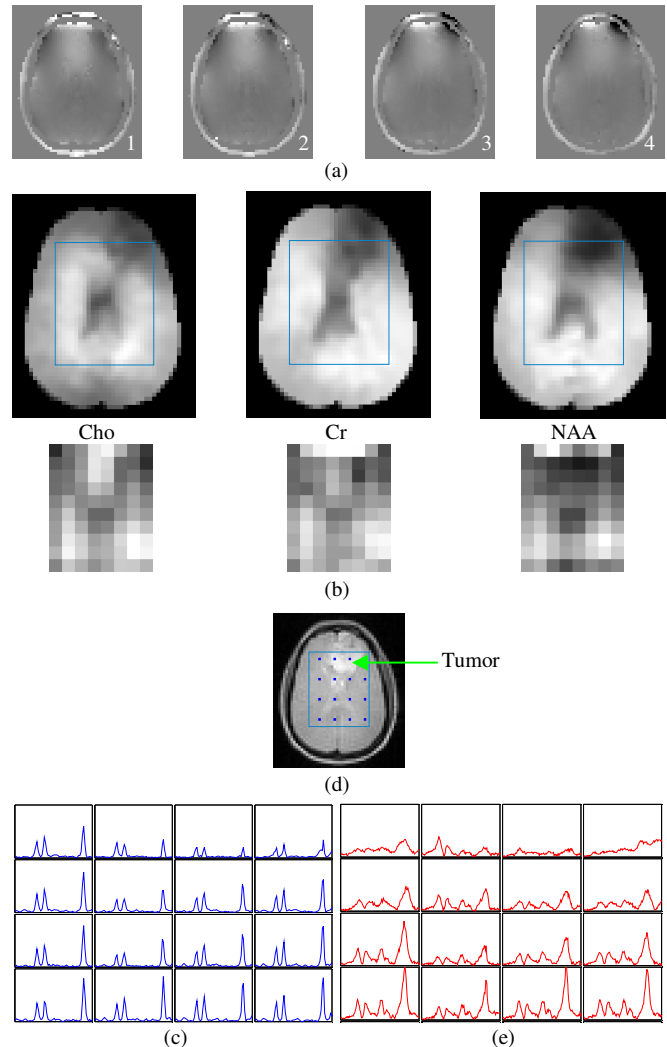


Fig. 4. (a) Estimated field map at four slices. The shown values are clipped between -80 and 80Hz. (b) Reconstructed peak maps of Cho, Cr, and NAA using the proposed method (Top row) and CSI method (Bottom row; corresponding to the same region indicated by a box in the top row). (c) A few spectral lines at voxels shown in (d) using the proposed method. (e) Spectra at the same voxels using the CSI scheme.

- hyperpolarized  $^{13}\text{C}$  flyback 3D-MRSI," *J. Mag. Res.*, vol. 192, no. 2, pp. 258-264, Jun. 2008.
- [4] A.A. Maudsley *et al.*, "Comprehensive processing, display and analysis for in vivo MR spectroscopic imaging," *NMR in biomedicine*, vol. 19, no. 4, pp. 492-503, 2006.